RESEARCH ARTICLE SUMMARY

IMMUNOLOGY

Marginal zone B cells acquire dendritic cell functions by trogocytosis

Patrick Schriek, Alan C. Ching, Nagaraj S. Moily, Jessica Moffat, Lynette Beattie, Thiago M. Steiner, Laine M. Hosking, Joshua M. Thurman, V. Michael Holers, Satoshi Ishido, Mireille H. Lahoud, Irina Caminschi, William R. Heath, Justine D. Mintern*, Jose A. Villadangos*

INTRODUCTION: Effective immunity is multilayered, requiring the cooperation of various types of molecules and cells. Some types are components of the fast-responding innate arm of the immune system, like the molecules that constitute the complement system and marginal zone (MZ) B cells. Other types of molecules and cells participate in adaptive immune responses that provide long-term protection. These include conventional dendritic cells (cDCs) and major histocompatibility complex class II (MHC II) molecules. This study describes molecular linkages between complement and MHC II molecules that enable MZ B cells and cDCs to carry out cooperatively immunological functions that neither cell type can perform on its own.

RATIONALE: The initiation of adaptive immunity against infections requires cDCs to detect, capture, degrade, and present pathogen antigens. cDCs use their MHC II molecules to bind and display peptide fragments derived from these antigens. Recognition of the resulting pMHC II complexes by the antigen receptor of T cells elicits adaptive immune responses and, eventually, the establishment of protective immunological memory against the infectious agent. MZ B cells are specialized in the production of polyreactive antibodies that protect newborns and infants from different types of microorganisms. In some instances, MZ B cells require "help" from T cells to perform this function, which they obtain by displaying pMHC II complexes. This suggests that MZ B cells may be able to emulate the antigen-presenting activity of cDCs.

RESULTS: Complement component 3 (C3) is an abundant serum protein that constitutively adopts a reactive form in the absence of pathogens by a mechanism known as tickover. We determined that C3 binds to pMHC II exposed on the surface of mouse and human cDCs, forming a covalent bond with the carbohydrate moiety of the MHC II α chain. Because C3 can damage healthy cells, it is converted to inactive C3dg while still bound to pMHC II. These pMHC II–C3dg complexes are recognized by complement receptor 2 (CR2), which is highly expressed by MZ B cells. Interaction between CR2 and C3dg triggers the transfer of pMHC II–C3dg complexes, along with associated cDC membrane and additional proteins embedded in the membrane, from cDCs to MZ B cells—a process termed trogocytosis. The trogocytic MZ B cells are thus able to present pMHC II complexes to T cells they do not generate themselves but acquire from cDCs.

Although trogocytosis is beneficial for MZ B cell function, it must be limited to prevent excessive damage and elimination of the trogocytosed cDCs. This takes place through an evolutionarily conserved mechanism, namely pMHC II–C3dg ubiquitination by a highly specialized ubiquitin ligase, MARCH1, embedded in the cDC plasma membrane. The ubiquitinated pMHC II–C3dg complexes are endocytosed and degraded intracellularly, reducing the number exposed on the cDC surface in the steady state.

CONCLUSION: Our results describe how C3 and MHC II interact and how this interaction enables MZ B cells and cDCs to cooperatively carry out functions they cannot perform individually. We demonstrate how an evolutionarily conserved mechanism for the constitutive elimination of potentially damaging C3 has been co-opted by cDCs to tag pMHC II complexes for capture by MZ B cells via trogocytosis. This mechanism expands the range of antigens that MZ B cells can present to T lymphocytes. The beneficial and deleterious consequences of trogocytosis are balanced by MARCH1 ubiquitination. ■

MHC II–C3dg complex formation and ubiquitination at the surface of cDCs

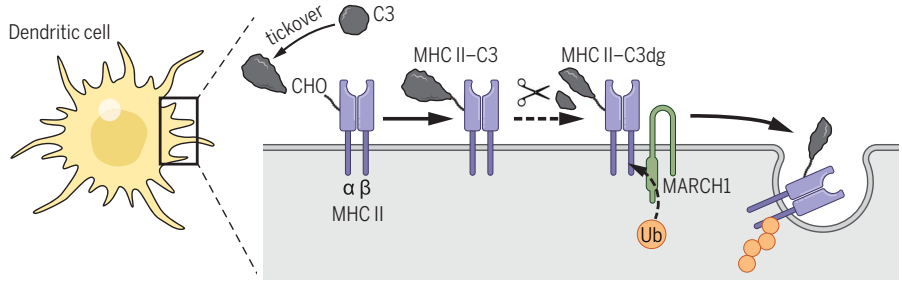

MZ B cells trogocytose from cDC pMHC II–C3 complexes for antigen presentation to CD4⁺ T cells

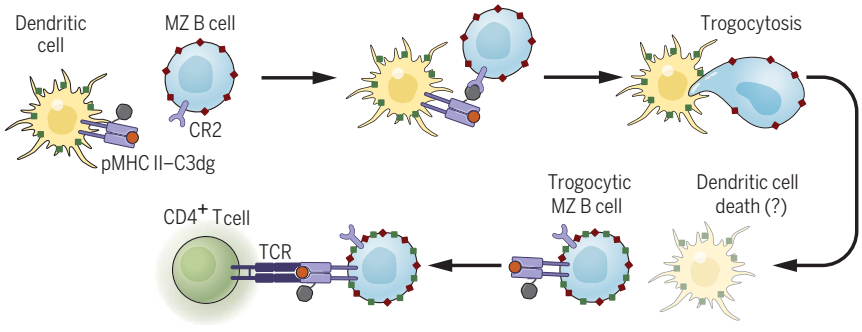

Marginal zone B cells trogocytose dendritic cells, acquiring peptide-loaded MHC II molecules bound to complement C3 for antigen presentation to CD4⁺ T cells. Activated complement C3 binds MHC II on conventional dendritic cells (cDCs). The complexes are processed into MHC II–C3dg and either internalized via MARCH1-mediated ubiquitination or recognized by the complement receptor 2 (CR2) of marginal zone (MZ) B cells. The latter enables MZ B cells to trogocytose and display on their own membrane cDC receptors. Trogocytic MZ B cells expand their capacity to stimulate helper CD4⁺ T cells using antigen-loaded MHC II molecules generated by cDCs. Excessive trogocytosis eliminates cDCs, but MARCH1 prevents this by limiting the number of MHC II–C3dg complexes on cDCs.

The list of author affiliations is available in the full article online.
*Corresponding author. Email: jmintern@unimelb.edu.au (J.D.M.); j.villadangos@unimelb.edu.au (J.A.V.)
Cite this article as P. Schriek *et al.*, *Science* **375**, eabf7470 (2022). DOI: 10.1126/science.abf7470

READ THE FULL ARTICLE AT
https://doi.org/10.1126/science.abf7470

RESEARCH ARTICLE

IMMUNOLOGY

Marginal zone B cells acquire dendritic cell functions by trogocytosis

Patrick Schriek[1], Alan C. Ching[1], Nagaraj S. Moily[1], Jessica Moffat[1], Lynette Beattie[2], Thiago M. Steiner[2], Laine M. Hosking[3], Joshua M. Thurman[4], V. Michael Holers[4], Satoshi Ishido[5], Mireille H. Lahoud[6], Irina Caminschi[6], William R. Heath[2], Justine D. Mintern[1]*, Jose A. Villadangos[1,2]*

Marginal zone (MZ) B cells produce broad-spectrum antibodies that protect against infection early in life. In some instances, antibody production requires MZ B cells to display pathogen antigens bound to major histocompatibility complex class II (MHC II) molecules to T cells. We describe the trogocytic acquisition of these molecules from conventional dendritic cells (cDCs). Complement component 3 (C3) binds to murine and human MHC II on cDCs. MZ B cells recognize C3 with complement receptor 2 (CR2) and trogocytose the MHC II–C3 complexes, which become exposed on their cell surface. The ubiquitin ligase MARCH1 limits the number of MHC II–C3 complexes displayed on cDCs to prevent their elimination through excessive trogocytosis. Capture of C3 by MHC II thus enables the transfer of cDC-like properties to MZ B cells.

Effective immunity requires orchestrated cooperation of multiple molecular and cellular components to maintain homeostasis and respond to infections. Although major histocompatibility complex class II (MHC II) molecules and complement component 3 (C3) are ancient centerpieces of adaptive and innate immunity, respectively, no interaction between these two components has previously been described.

The primary role of MHC II is to bind peptides derived from protein antigens (Ag) encountered by antigen-presenting cells (APCs) (*1*). The resulting peptide-loaded MHC II (pMHC II) complexes are displayed on the APC plasma membrane and detected by $CD4^+$ T cells, initiating adaptive immune responses. All APCs ubiquitinate the cytosolic tail of MHC II using the membrane ubiquitin ligase MARCH1 (membrane-associated RING-CH–type finger 1, encoded by *March1*) (*2*). Ubiquitination reduces the surface expression and half-life of pMHC II complexes by promoting their delivery to lysosomes, where they are degraded (*2*). Both MARCH1 and the single MHC II β-chain residue ubiquitinated by MARCH1, Lys^{225}, have been conserved through evolution, but their role in Ag presentation remains elusive (*2*–*4*), raising questions as to whether MHC II ubiquitination by MARCH1 plays other functions.

The complement system comprises >30 soluble and membrane proteins that undergo a cascade of activation upon pathogen encounter (*5*). Its pivotal component is C3, which can be activated by the classical, lectin, or alternative pathways (fig. S1A). This third pathway occurs at low levels in the absence of pathogens in what is known as tickover. Activated C3 binds covalently to carbohydrates on bacterial cell walls (*6*). This is followed by recruitment of other complement components that mediate lysis or phagocytosis of bacteria (fig. S1A) (*5*). C3 can also bind to the plasma membrane of normal host cells during and, via tickover, in the absence of infection (*6*). Deposited C3 is recognized by surface receptors and serum proteases that cleave it into the inactive forms C3dg and C3d, which remain attached to the cell membrane (fig. S1, B and C, and table S1), thereby preventing cell damage. Activation of C3 by tickover primes the complement system to respond rapidly to infection, but whether this pathway plays other immunoregulatory roles in the steady state is unclear (*7*).

Here, we show that C3 activated by tickover specifically binds the carbohydrate of murine and human MHC II glycoproteins. The resulting complexes are recognized by complement receptor 2 (CR2), expressed by marginal zone (MZ) B cells, triggering the trogocytic transfer of pMHC II and other membrane proteins from conventional dendritic cells (cDCs) to MZ B cells. This mechanism enables MZ B cells to present pMHC II complexes generated by cDCs. Excessive trogocytosis causes cDC elimination, but MARCH1 ubiquitination prevents this outcome by limiting the accumulation of MHC II–C3 complexes.

[1]Department of Biochemistry and Pharmacology, Bio21 Molecular Science and Biotechnology Institute, University of Melbourne, Parkville, VIC 3010, Australia. [2]Department of Microbiology and Immunology, Peter Doherty Institute for Infection and Immunity, University of Melbourne, Parkville, VIC 3010, Australia. [3]Department of Allergy and Immunology, Royal Children's Hospital, Parkville, VIC 3052, Australia. [4]Division of Rheumatology, University of Colorado School of Medicine, Aurora, CO 80045, USA. [5]Department of Microbiology, Hyogo College of Medicine, 1-1 Mukogawa-cho, Nishinomiya 663-8501, Japan. [6]Monash Biomedicine Discovery Institute and Department of Biochemistry and Molecular Biology, Monash University, Clayton, VIC 3800, Australia.
*Corresponding author. Email: jmintern@unimelb.edu.au (J.D.M.); j.villadangos@unimelb.edu.au (J.A.V.)

March1$^{-/-}$ mice have reduced numbers of splenic cDCs

Relative to wild-type controls, the spleens of *March1*$^{-/-}$ mice exhibited reduced numbers of the two major cDC subsets, cDC1s and cDC2s, with no alteration in the number of plasmacytoid DCs (pDCs), B cells, or T cells (Fig. 1, A and B, and fig. S2, A to C). By contrast, cDC numbers in lymph nodes and the thymus were not altered (fig. S2D). The expression of characteristic cDC markers was comparable between wild-type and *March1*$^{-/-}$ cDCs with the exception of the MARCH1 substrates MHC II and CD86 (fig. S2E).

March1$^{-/-}$ mice have enriched numbers of MZ B cells displaying cDC proteins

A splenic $CD11c^{int}CD24^+CD8^{int}$ population that was present in low numbers in wild-type mice comprised >20% of $CD11c^+$ cells in their *March1*$^{-/-}$ counterparts (Fig. 2A). These cells displayed several surface markers characteristic of cDC1s, cDC2s, or both, although mostly at lower levels than cDCs (Fig. 2B). They also expressed B cell molecules at levels similar to B cells but did not express markers characteristic of other cell populations (Fig. 2B). No equivalent cell type was found in lymph nodes or thymus (fig. S3A). The transcriptome of $CD11c^{int}CD24^+CD8^{int}$ cells was similar to those of wild-type or *March1*$^{-/-}$ B cells (Fig. 2C), with high expression of B cell receptor (BCR)–signaling and B cell–activation genes (Fig. 2D) and no expression of cDC genes (Fig. 2E). This suggested that $CD11c^{int}CD24^+CD8^{int}$ cells were B cells that displayed cDC surface proteins but did not transcribe the corresponding genes. Additional immunophenotyping revealed that the majority of these cells were MZ B cells (*8*) (Fig. 2F).

MZ B cells trogocytose plasma membrane from cDCs in a MARCH1-dependent manner

We tested the hypothesis that MZ B cells displayed cDC membrane proteins as a result of trogocytosis (*9*–*11*) and the absence of MARCH1-promoted plasma membrane transfer between the two cell types (fig. S3B). Indeed, B cells incubated with cDCs trogocytosed fluorescently labeled plasma membrane (Fig. 3A) and surface receptors (Fig. 3B) from cDCs. Trogocytosis was more prominent if cDCs were *March1*$^{-/-}$ than if they were wild-type, even though the two cDC groups were similarly labeled with fluorescent membrane dye (fig. S3C) and expressed similar levels of the surface receptors acquired by the B cells (fig. S2E). Membrane transfer between cDCs and B cells was monodirectional, as little

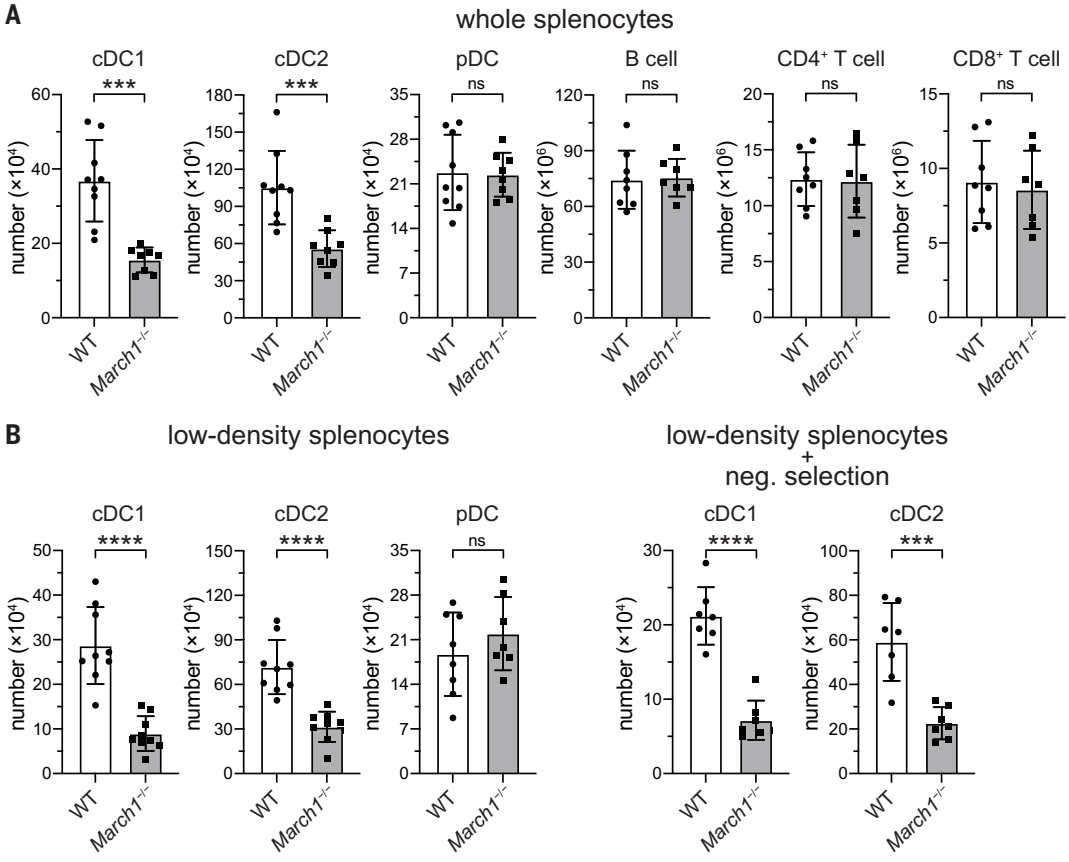

Fig. 1. Mice deficient in MARCH1 E3 ubiquitin ligase have reduced numbers of splenic cDCs. (**A** and **B**) Numbers of the indicated wild-type (WT) and *March1*$^{-/-}$ cell types in whole splenocytes (A) or low-density splenocyte preparations (B) before (left) and after (right) depletion of non-cDCs. Graphs display data pooled from three independent experiments, with each symbol representing an individual mouse (n = 2 or 3 per experiment); bars denote mean ± SD. ***P < 0.0002, ****P < 0.0001 [independent-samples t test with Welch's correction (no assumption of equal variances), two-tailed P value (95% CI)]; ns, not significant.

transfer was observed from B cells to cDCs (fig. S3D). MZ B cells were more trogocytic than their follicular (FO) counterparts (Fig. 3C). Furthermore, B cells did not trogocytose *March1*$^{-/-}$ macrophage, neutrophil, or T cell membranes (fig. S3E). Thus, B cells—particularly MZ B cells—specifically acquire cDC plasma membrane and surface proteins via trogocytosis, and MARCH1 deficiency makes cDC membranes more susceptible to trogocytic transfer.

MARCH1 controls the amount of C3 that accumulates on the surface of cDCs

Trogocytosis is mediated by surface receptors (*9*), so we hypothesized that MARCH1 regulates the expression of a receptor that mediates trogocytosis. The only receptors known to increase in expression in *March1*$^{-/-}$ cDCs are MHC II and CD86 (fig. S2E) (*2*), but a recent plasma membrane proteome analysis showed that the surface of *March1*$^{-/-}$ cDCs is also highly enriched in C3 (*12*). Because C3 is inaccessible to cytosolic ubiquitination by MARCH1, we sought to characterize the mechanism that caused its accumulation on the cell surface before investigating its potential role in trogocytosis.

First, we confirmed that C3 is present on wild-type cDC1s and cDC2s and is overexpressed on their *March1*$^{-/-}$ counterparts (Fig. 4A and fig. S4A). Analysis of C3-deficient mice demonstrated the specificity of this detection (Fig. 4A). MARCH1 is active in all hematopoietic APCs, where it keeps surface MHC II expression at intermediate to low levels (*12*). We observed an increase in C3 deposition on both professional and "atypical" APCs from the spleen, lymph nodes, and thymus but not on T cells (Fig. 4B). C3 binding to cDCs was not caused by enzymatic tissue digestion because it was also observed in cell suspensions prepared by mechanical disruption (fig. S4B). Furthermore, when wild-type and *March1*$^{-/-}$ × *C3*$^{-/-}$ spleens were pooled before cell purification, the mutant cDCs remained negative for C3 expression (fig. S4C).

In mixed–bone marrow (BM) chimeric mice where 1:1 wild-type and *March1*$^{-/-}$ BM was used to reconstitute *C3*$^{-/-}$ recipients, neither wild-type nor *March1*$^{-/-}$ cDCs displayed C3 (Fig. 4C). This indicated that C3 was captured from the extracellular environment, as expected, because it is produced mainly by liver cells (*13*). If the recipient chimeric mice were wild-type, the cDCs generated from the *March1*$^{-/-}$ BM displayed higher surface expression of C3 than their wild-type counterparts (Fig. 4C), which implies that the effect of the mutation was cell-intrinsic. Thus, C3 is secreted into circulation by nonhematopoietic cells and is deposited on all APCs. If the cells do not express MARCH1, C3 deposition increases by as much as a factor of 20 in the case of cDC1s.

C3 activated by tickover binds to MHC II

Proteomic analysis of the *March1*$^{-/-}$ cDC plasma membrane (*12*) (table S2) indicated that the C3 species found on the cDC surface is one or both of its inactivated forms (i.e., C3dg or C3d) (fig. S1B and table S1). Analysis of wild-type, *March1*$^{-/-}$, and *C3*$^{-/-}$ cDC lysates by immunoblot identified several molecular species of C3 that were only detected in *March1*$^{-/-}$ cDCs (Fig. 5A, fig. S1B, and table S1). The most prominent species had a molecular weight of ~70 kDa and was absent from the serum. We hypothesized that this species corresponded to C3dg or C3d covalently bound to MHC IIα or β.

The cDCs of mice deficient in both MARCH1 and MHC II (*March1*$^{-/-}$ × *H2-Aa*$^{-/-}$) showed elevated CD86 expression (fig. S4D), indicating that the absence of MHC II did not prevent surface accumulation of MARCH1 substrates. However, C3 was barely detectable on the surface of these cells (Fig. 5B) or on cDCs that only lacked MHC II expression (fig. S4E). Furthermore, the cDCs of knock-in mice—in which the only MHC II ubiquitination site, Lys^{225} of the β chain, has been replaced with Arg (MHC IIKR$^{KI/KI}$ mice) (*3*, *14*)—expressed similarly high levels of C3 relative to *March1*$^{-/-}$

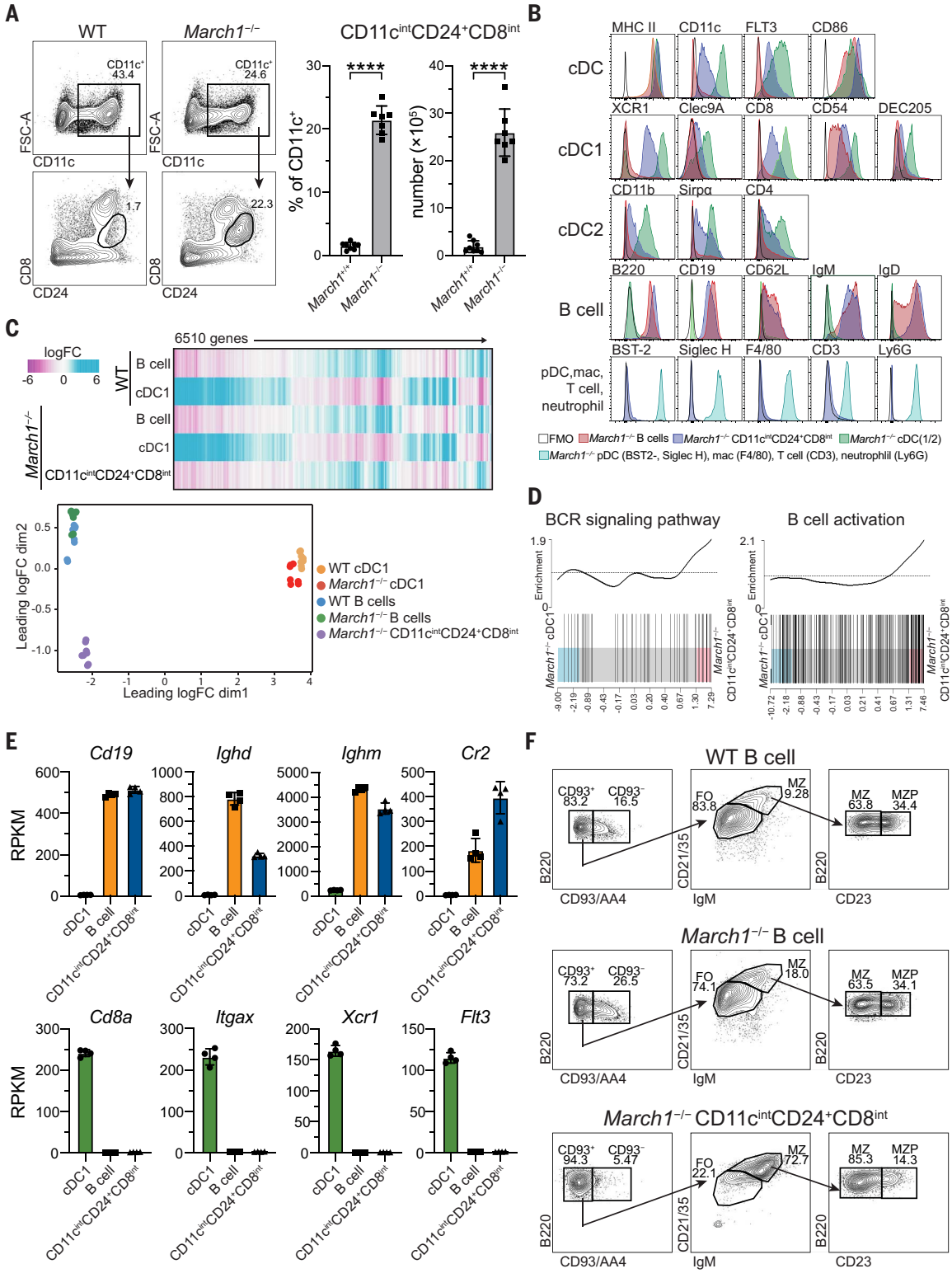

Fig. 2. MARCH1-deficient mice harbor MZ B cells expressing cDC surface proteins. (**A**) Left: Representative flow cytometry plots of CD24 versus CD8 expression in CD11c$^+$ wild-type and *March1*$^{-/-}$ low-density splenocytes. Right: Frequencies and total numbers of CD11c^{int}CD24$^+$CD8^{int} cells. Graphs display data pooled from three independent experiments, with each symbol representing an individual mouse (n = 2 or 3 per experiment); bars denote mean ± SD. ****P < 0.0001 [independent-samples t test with Welch's correction (no assumption of equal variances), two-tailed P value (95% CI)]. (**B**) Flow cytometry analysis of the indicated surface molecules on splenic CD11c^{int}CD24$^+$CD8^{int} cells (blue), cDCs (green), or B cells (red) of *March1*$^{-/-}$ mice. Histograms are representative of at least two independent experiments with two or three individual mice per experiment. (**C** to **E**) RNA-seq of sort-purified CD11c^{int}CD24$^+$CD8^{int} cells from *March1*$^{-/-}$ mice and B cells and cDC1s from wild-type and *March1*$^{-/-}$ mice. (C) Top: Heatmap showing 6510 differentially expressed genes across the five groups. Bottom: Two-dimensional scaling plot of the top 500 differentially expressed genes. (D) Barcode plots showing enrichment of genes in the B cell receptor signaling pathway (BioCarta) (left) and B cell activation (GO:0042113) (right) based on gene set analysis comparing *March1*$^{-/-}$ CD11c^{int}CD24$^+$CD8^{int} cells and cDC1s. (E) Reads per kilobase million (RPKM) for genes encoding characteristic B cell (top) or cDC1 (bottom) surface markers in *March1*$^{-/-}$ cDC1s, B cells, and CD11c^{int}CD24$^+$CD8^{int} cells. For RNA-seq analysis in (C) to (E), mRNAs from sort-purified cells of four biological replicates with pooled spleens from five mice were sequenced in technical replicates. (**F**) Representative gating strategy for the identification of splenic follicular (FO), MZ, and progenitor MZ (MZP) B cells, based on the surface expression of B220, CD93, IgM, CD21/35, and CD23 (all gated on CD19$^+$ alive cells), in whole splenocyte preparations of wild-type and *March1*$^{-/-}$ mice (top and middle rows) or among the CD11c^{int}CD24$^+$CD8^{int} cells from low-density splenocytes of *March1*$^{-/-}$ mice (bottom). Data are from at least two independent experiments with two or three individual mice per experiment.

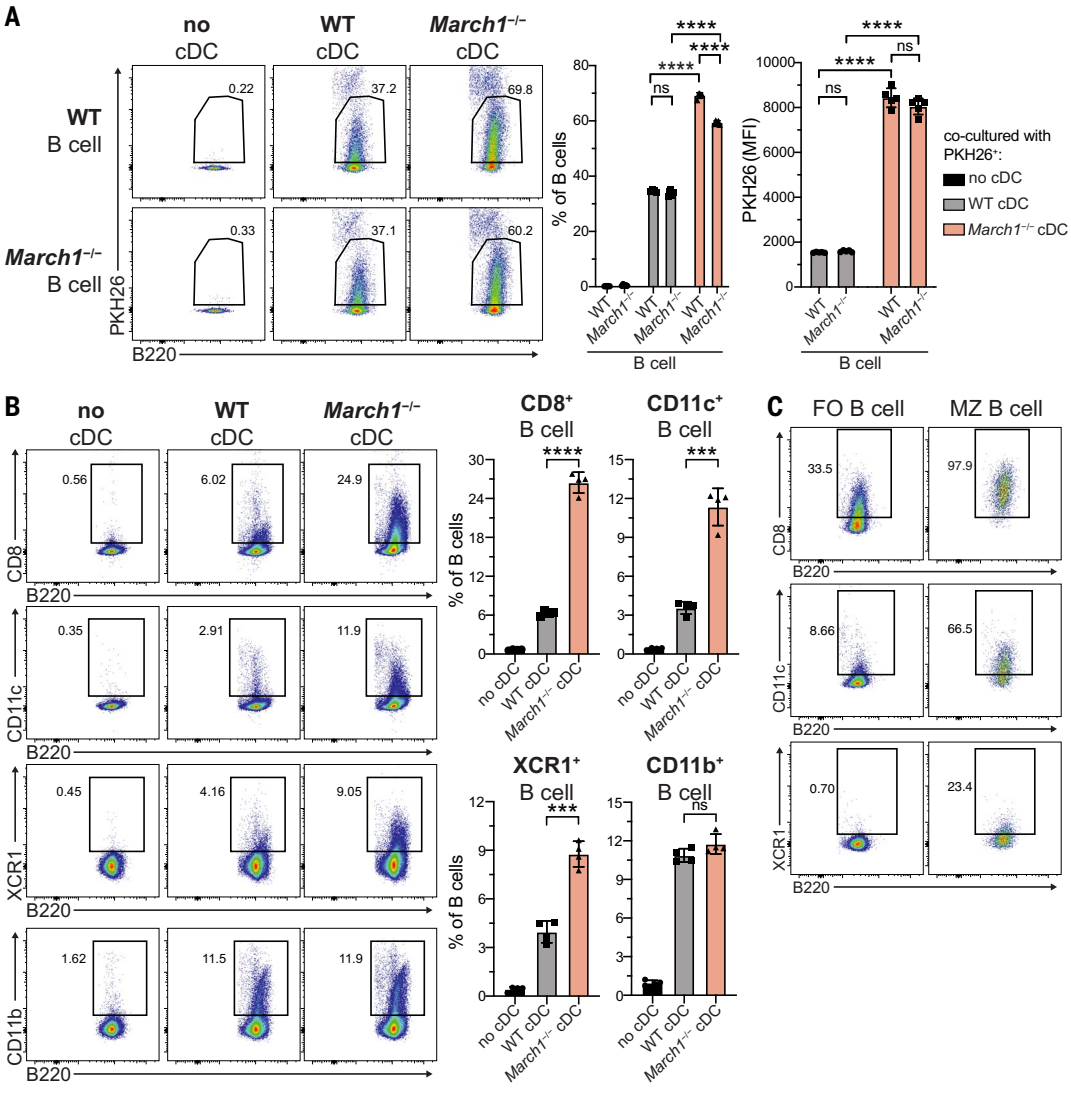

Fig. 3. MZ B cells trogocytose cDC plasma membrane in vitro. (**A**) Left: Trogocytic acquisition of cDC membrane, fluorescently labeled with PKH26, by wild-type and *March1*$^{-/-}$ B cells after in vitro incubation with PKH26-stained wild-type or *March1*$^{-/-}$ cDCs. Right: Frequency of PKH26^{+} B cells and the mean fluorescence intensity (MFI) value of their PKH26 fluorescence after coculturing. (**B**) As in (A), but measuring the indicated cDC proteins. (**C**) As in (B), but displaying separately FO and MZ B cells (as identified in Fig. 2F). Graphs in (A) and (B) display data pooled from two independent experiments, with each data point (n = 2 or 3 per experiment) representing a measurement of a technical replicate; bars denote mean ± SD. ***P < 0.0002, ****P < 0.0001 [Welch's analysis of variance (ANOVA) test (no assumption of equal variances) followed by pairwise comparison (A) or by Games-Howell multiple-comparisons test (B), adjusted P value (95% CI)]. Plots in (C) are representative of at least two independent experiments with two or three individual mice per experiment.

cDCs (Fig. 5B), even though MARCH1 is functional in these cells as shown by their wild-type expression of CD86 (fig. S4F).

To confirm the formation of MHC II–C3 complexes in cDCs, we immunoprecipitated MHC II or C3 from wild-type, *March1*$^{-/-}$, *March1*$^{-/-}$ × *C3*$^{-/-}$, MHC IIKR$^{KI/KI}$, *C3*$^{-/-}$, and *H2-Aa*$^{-/-}$ cDCs and detected MHC IIα, MHC IIβ, and C3 by immunoblot. Two ~70-kDa proteins recognized by anti–I-Aα and anti-C3 but not by anti–I-Aβ antibodies were identified in immunoprecipitates from *March1*$^{-/-}$ and MHC IIKR$^{KI/KI}$ cells, but not from *C3*$^{-/-}$ cells (Fig. 5, C and D). Mass spectrometry analysis of this protein confirmed that it contained C3d/C3dg peptides (table S3). Accumulation of C3 on cDC1s was accompanied by increased expression of complement regulators involved in conversion of C3b to C3dg, namely CR1/CR2, complement decay-accelerating factor (DAF), and factor H (fig. S4G). Thus, activated C3 binds to I-Aα; it is then processed, generating I-Aα–C3dg and I-Aα–C3d complexes, which accumulate on the surface of APCs (fig. S1D). For simplicity, we henceforth use the term "C3dg" to refer to both C3d and C3dg isoforms.

A comparison of C3 levels on the surface of cDCs expressing wild-type, MHC II K225R mutant molecule, or no MHC II at all (*H2-Aa*$^{-/-}$) indicated that virtually all C3 was associated with MHC II (Fig. 5B and fig. S4E). This suggested that some feature in the MHC IIα glycoprotein made it a target for activated C3. Activated C3 displays little protein conformation specificity but reacts preferentially with mannose (*6*), so we explored the possibility that C3dg might be bound to the MHC IIα carbohydrate. Indeed, when MHC II immunoprecipitated from *March1*$^{-/-}$ cDCs was deglycosylated with PNGase F, the MHC IIα–C3dg complex was not detectable (Fig. 5E). This was accompanied by a change in free I-Aα mobility in SDS–polyacrylamide gel electrophoresis due to the loss of the carbohydrate group (Fig. 5E).

Binding of C3 to MHC II is conserved in mice and humans

To test whether C3 binding to MHC II was a peculiarity of C57BL/6 mice, we measured C3 on cDCs of *March1*$^{-/-}$ mice backcrossed to BALB/c (H-2^{d} haplotype) or C3H (H-2^{k} haplotype) mice. High levels of C3 were present on cDCs of all three strains (fig. S5A). We also detected C3 on human blood DCs (fig. S5, B and C), with highest expression on cDC2s followed by pDCs and cDC1s (Fig. 6). To determine whether C3 binding required MHC II expression, we assessed DCs in parallel from two human donors with a 362A>T mutation in RFXANK, which causes impaired MHC II transcription (*15*) and a lack of MHC II at the cell surface (fig. S5B). All MHC II–deficient DCs showed reduced C3 expression (Fig. 6). Thus, like MHC II ubiquitination by MARCH1, constitutive C3

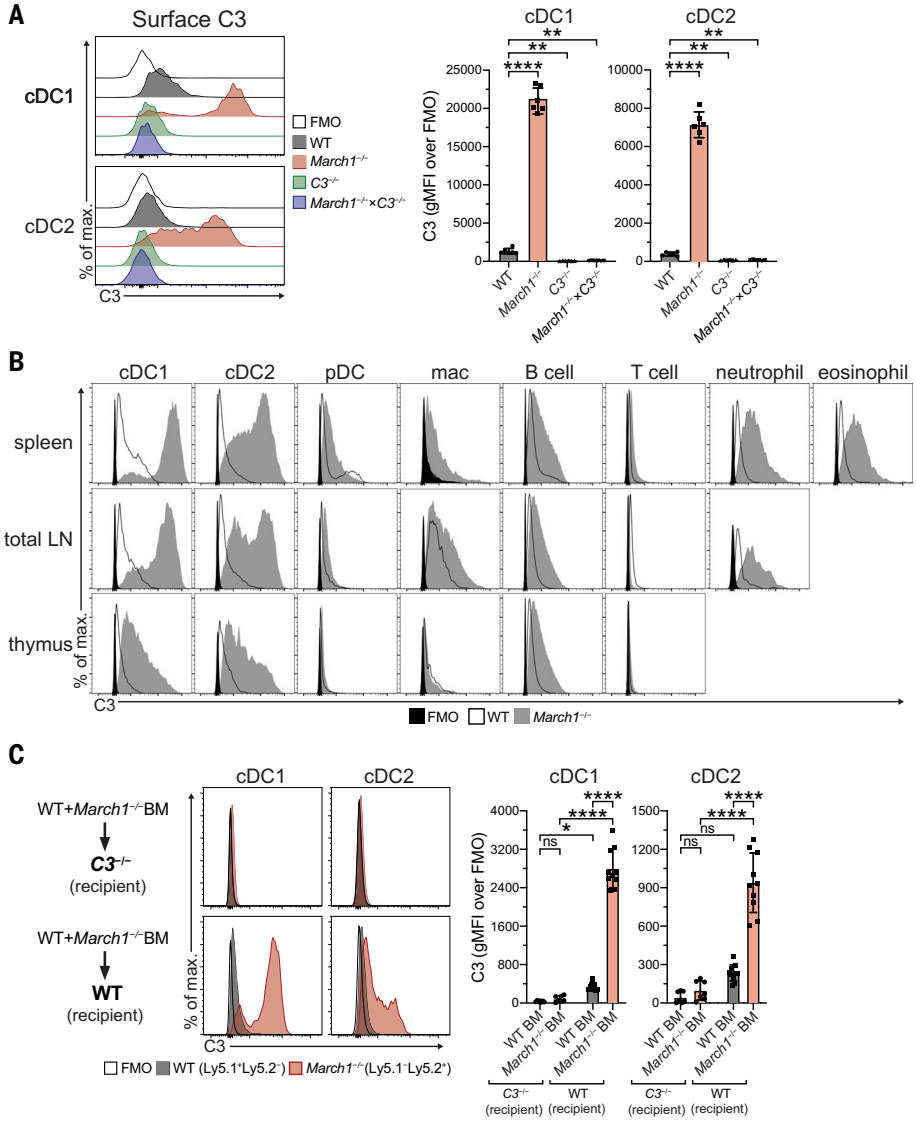

Fig. 4. Complement C3 deposition on the surface of splenic cDCs. (**A**) Representative flow cytometry histograms (left) and bar graphs with MFI values (right) of C3 surface expression on splenic cDC1s and cDC2s purified from the indicated mice. (**B**) Representative histograms of flow cytometry analysis of C3 surface levels on the indicated cell types in spleen, lymph nodes (LN), and thymus of wild-type or *March1*$^{-/-}$ mice. Histograms are representative of at least two independent experiments with two or three individual mice per experiment. (**C**) Representative flow cytometry histograms (left) and bar graphs with MFI values (right) of C3 surface expression on wild-type and *March1*$^{-/-}$ cDC1s and cDC2s from mixed-BM chimeras where wild-type or *C3*$^{-/-}$ recipient mice were reconstituted with a 1:1 mix of wild-type and *March1*$^{-/-}$ BM. Graphs in (A) and (C) display data pooled from a minimum of two independent experiments, with each symbol representing an individual mouse (n = 3 to 5 per experiment); bars denote mean ± SD. *P < 0.0332, **P < 0.002, ****P < 0.0001 [Welch's ANOVA test (no assumption of equal variances) followed by Games-Howell multiple-comparisons test (A) or by pairwise comparison (C), adjusted P value (95% CI)].

binding to MHC II has been conserved through evolution.

CR2 drives B cell trogocytosis of cDC membranes containing MHC II–C3 complexes

Analysis in vitro confirmed that high surface MHC II–C3 expression on MHC IIKR$^{KI/KI}$ cDCs was necessary and sufficient to induce B cell trogocytosis (Fig. 7A and fig. S6A). C3dg is the ligand for complement receptor 2 (CR2, also known as CD21), which is expressed only by B cells (*5*). CR2-deficient B cells lacked the capacity to trogocytose more membrane from C3-decorated cDCs than from wild-type cDCs (Fig. 7A and fig. S6A). Furthermore, MZ B cells express higher levels of CR2 than FO B cells (Fig. 2F), and virtually all MZ B cells trogocytosed cDC membrane containing MHC II–C3dg complexes (fig. S6B).

We next tested the validity of the conclusions from our in vitro analyses in vivo. *March1*$^{-/-}$ and MHC IIKR$^{KI/KI}$ mice accumulated trogocytic (CD8^{+}CD11c^{+}) B cells in their spleens in a MHC II– and C3-dependent manner (Fig. 7B). Wild-type spleens contained a small number of CD8^{+}CD11c^{+} MZ B cells, but these were absent from *C3*$^{-/-}$ spleens (Fig. 7C and fig. S6C); hence, trogocytosis occurred constitutively in wild-type mice. Although lymph node cDCs also displayed MHC II–C3 complexes (Fig. 4B), few trogocytic B cells were detected in lymph nodes (fig. S6D), as expected because mouse lymph nodes lack MZ B cells (*8*). The number of splenic cDCs decreased in all mice where cDCs had enriched C3 surface expression (Fig. 7D) and B cells expressed CR2 (Fig. 7E), in lockstep with the increase in trogocytic MZ B cells. The spleens of mice deficient in C3 did not contain more cDCs than those of wild-type mice (fig. S6E); this finding suggests that the limited amount of trogocytosis occurring in wild-type mice is insufficient to affect cDC homeostasis.

To further assess whether cDC number reduction and trogocytosis were directly correlated, we produced mixed-BM chimeras where wild-type or *C3*$^{-/-}$ recipient mice were reconstituted with 1:1 wild-type and *March1*$^{-/-}$ BM. In wild-type recipient mice, both wild-type and *March1*$^{-/-}$ B cells displayed higher trogocytic activity, but only *March1*$^{-/-}$ cDCs were reduced in numbers. Neither of these events were observed in C3-deficient recipients (Fig. 7F). Thus, the loss of cDCs required the accumulation of MHC II–C3 complexes but was caused by CR2-dependent MZ B cell trogocytosis (fig. S7).

Trogocytic MZ B cells present pMHC II generated by cDCs

Because the primary mediator of trogocytic cDC membrane transfer to B cells was CR2 recognition of MHC II–C3dg complexes, we wondered whether the complexes found on splenic B cells (Fig. 4B) were in fact acquired from cDCs. In mixed-BM chimeras where wild-type recipient mice were reconstituted with a 1:1 mix of wild-type and *Cr2*$^{-/-}$ BM, all B cells, and in particular MZ B cells, displayed more C3 if they expressed CR2 than if they did not (Fig. 8A). This suggested that although some of the MHC II–C3 complexes displayed by B cells probably formed on the B cells themselves, most were acquired from cDCs. This is supported by the absence of C3 detection on B cells of mice where MHC II–C3 complexes could not be generated (i.e., *H2-Aa*$^{-/-}$) or lacked CR2 expression (Fig. 8B), which indicates that virtually all C3 (bound to MHC II) on the B cell surface was acquired by trogocytosis of cDCs. These results also confirmed that

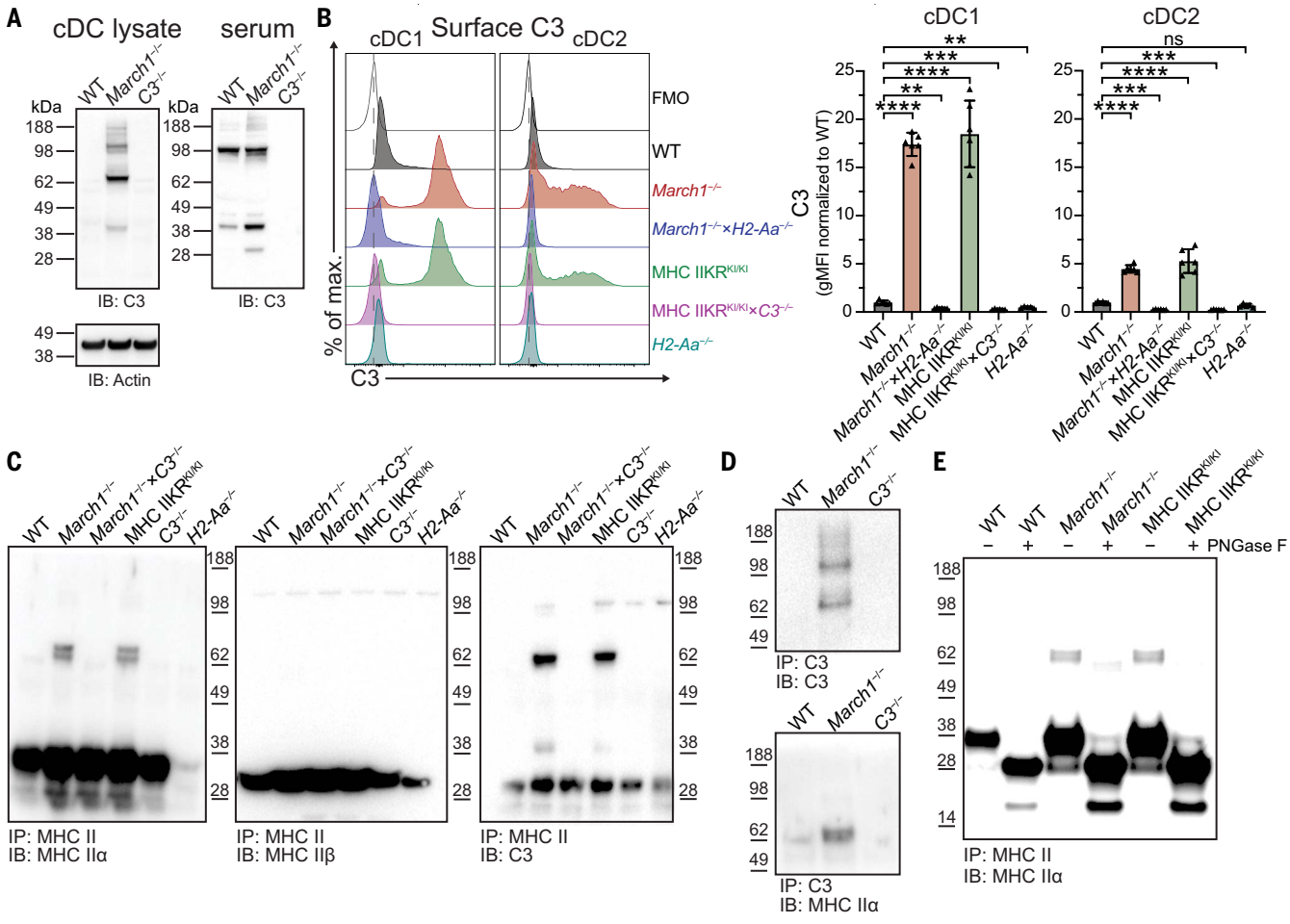

Fig. 5. C3 binds covalently to the MHC IIα carbohydrate on the surface of cDCs. (**A**) Immunoblot (IB) of C3 from lysates of splenic cDCs and serum of wild-type, *March1*$^{-/-}$, or *C3*$^{-/-}$ mice. (**B**) Representative flow cytometry histograms (left) and bar graphs with MFI values (right) of C3 surface expression on splenic cDC1s and cDC2s of the indicated wild-type and mutant mice. Graphs display normalized data pooled from two independent experiments, with each symbol representing an individual mouse (n = 3 per experiment); bars denote mean ± SD. $^{**}P < 0.002$, $^{***}P < 0.0002$, $^{****}P < 0.0001$ [Welch's ANOVA test (no assumption of equal variances) followed by Games-Howell multiple-comparisons test, adjusted P value (95% CI)]. (**C**) IB analysis of MHC II immunoprecipitates (IPs) obtained from lysates of cDC1s of the indicated wild-type or mutant mice, using Abs against MHC IIα, MHC IIβ, or C3. (**D**) IB detection of MHC IIα in IPs of C3 obtained from cDC1 lysates of the indicated wild-type or mutant mice. (**E**) IB analysis of MHC II IPs obtained from cDC1 lysates of the indicated wild-type or mutant mice after treatment with (+) or without (−) PNGase F and subsequent detection of MHC IIα. All immunoblots in (C) to (E) derive from separate gels and membranes for each immunoblot (instead of sequential detection) and are representative of at least three independent experiments, each lane loaded with IPs from cell lysate of 2.5 × 10^5 purified splenic cDCs.

MZ B cell trogocytosis occurs constitutively in wild-type mice.

Finally, we tested whether trogocytosis enabled MZ B cells to "hijack" cDC Ag-presenting functions by acquiring pMHC II complexes generated by cDCs. First, we assessed MZ B cell presentation of the model Ag, I-Ea$_{46\text{-}72}$ (IEpep) (*16*), after cDC1-targeted immunization. Wild-type, MHC IIKR$^{KI/KI}$, and MHC IIKR$^{KI/KI}$ × *C3*$^{-/-}$ mice were immunized with an Ag consisting of IEpep fused to either an isotype control monoclonal antibody (mAb) or a mAb that recognizes Clec9A, a cDC1 receptor (*17*). Presentation of IEpep bound to MHC II (I-A^b) was measured with a mAb (YAe) that specifically recognizes this complex (*16*) (Fig. 8C). In wild-type mice immunized with the mAb that binds Clec9A, only cDC1s, not cDC2s or B cells, presented IEpep (Fig. 8D). Additionally, no presentation occurred after immunization with the isotype control mAb (Fig. 8D). Immunization of MHC IIKR$^{KI/KI}$ and MHC IIKR$^{KI/KI}$ × *C3*$^{-/-}$ mice with the isotype control mAb led to low presentation of IEpep by all four cell types (Fig. 8D), which is likely due to their increased MHC II surface expression. However, immunization with Clec9A-targeted mAb led to a much higher IEpep presentation by cDC1s. This was the case in both MHC IIKR$^{KI/KI}$ and MHC IIKR$^{KI/KI}$ × *C3*$^{-/-}$ mice, implying that presentation of IEpep by cDC1 was C3-independent (Fig. 8D). By contrast, presentation of the epitope by MZ B cells was C3-dependent (Fig. 8D). This indicated that C3-mediated trogocytosis enabled MZ B cells to display in vivo pMHC II complexes they cannot generate on their own but can acquire from cDC1s. To assess whether acquired pMHC II complexes could be recognized by T cells, we immunized wild-type, MHC IIKR$^{KI/KI}$, and MHC IIKR$^{KI/KI}$ × *C3*$^{-/-}$ mice with Clec9A mAb conjugated to the model Ag ovalbumin (OVA). We purified splenic FO and MZ B cells and incubated them in vitro with I-A^b-OVA$_{323\text{-}339}$–specific transgenic T cells (OT-II). Only MHC IIKR$^{KI/KI}$ MZ and, to a lesser extent, FO B cells presented the antigen and hence stimulated OT-II cells (Fig. 8E).

Discussion

We have described two intersections between the innate and adaptive immune systems. The

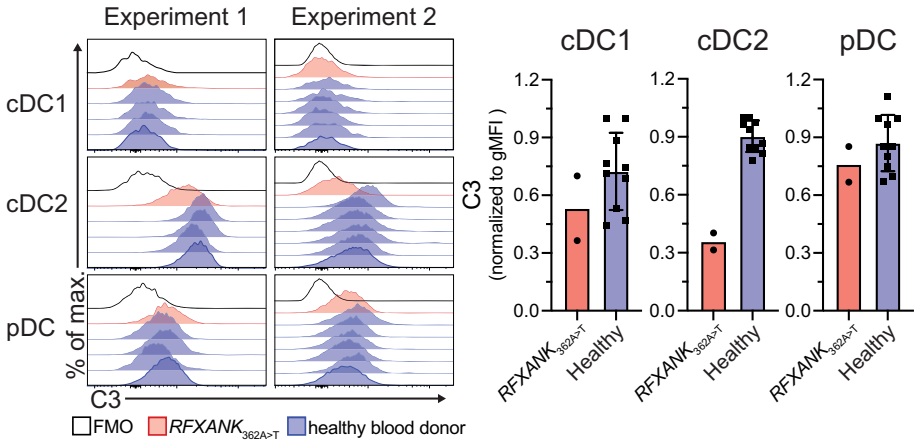

Fig. 6. MHC II–dependent C3 deposition on human blood dendritic cells. Representative flow cytometry histograms (left) and bar graphs with MFI values (right) of C3 surface expression on human blood DCs of healthy donors and two MHC II–deficient (*RFXANK*$_{362A>T}$) patients. Graphs display pooled data (normalized to highest geometric MFI values) from the two experiments, with each symbol representing an individual blood sample; bars denote mean ± SD.

first is cellular and features cDCs and MZ B cells. The main role of cDCs is to present Ag to T cells and initiate adaptive immunity (*18*). Interactions between cDCs and B cells are less well characterized (*19*). MZ B cells produce multispecific Abs that protect infants whose adaptive immune systems have not yet generated the full spectrum of memory B cells that differentiate from the FO B cell repertoire (*20*). This activity is considered to be T cell–independent. MZ B cells also engage in T cell–dependent immunity (*8*), but this requires Ag presentation, and it remains unclear whether MZ B cells are efficient APCs. Here, we demonstrated that MZ B cells are constitutively in contact with cDCs and acquire pMHC II complexes from them using C3- and CR2-dependent trogocytosis.

The second interaction between innate and adaptive immunity we have described occurs at the molecular level. Activation of C3 by tickover (in the absence of pathogen) "pre-charges" the complement system to respond to infection (*7*). However, activated C3 can bind to healthy cells and cause autoimmunity, and several mechanisms are in place to inactivate it (*6*). We showed that C3 activated by tickover binds to the MHC IIα carbohydrate. C3 is then converted to C3dg, and the resulting MHC II–C3dg complexes are ubiquitinated, internalized, and degraded (fig. S1D). Formation and ubiquitination of these complexes are independent processes conserved in mice and humans. Their role may be to prevent C3-driven host cell damage. We have not observed overt inflammation or autoimmunity in mice deficient in MHC II ubiquitination (*21*), but such disorders often do not manifest spontaneously in laboratory mice.

The MHC II carbohydrate appears to have a property that makes it prone to C3 binding and is not found in other glycoproteins; possibly this consists of a high mannose content (*6*). Because the proportion of MHC II molecules bound to C3 at any given time is small, only some molecules may carry the required carbohydrate. It is plausible that mannose removal is incomplete in a fraction of MHC II molecules passing through the Golgi complex, causing microheterogeneity as previously observed (*22*). Moreover, the size of this fraction may vary among cells as a result of differential expression of glycosidases (*23*), which would explain why cells with similar levels of surface MHC II (e.g., cDC1s, cDC2s, and B cells) displayed different amounts of C3.

Recognition of C3dg by CR2 was sufficient to trigger the trogocytic acquisition of cDC membrane by MZ B cells. The mechanism of trogocytosis is poorly understood (*11*). It can be driven by a single receptor-ligand interaction, as demonstrated here between C3dg on cDCs and CR2 on B cells, but it is unclear whether this interaction simply increases cell-cell adhesion or triggers active membrane transfer. Regardless, we showed that B cell trogocytosis of cDC1s occurs in wild-type mice and enables MZ B cells to present pMHC II complexes generated by cDC1s. These results help to explain how MZ B cells may modulate T cell–dependent responses. In addition, trogocytic B cells acquired other cDC receptors that may expand the range of MZ B cell functions—for instance, capture of Ag recognized by SIGN-R1, Clec9A, and other receptors (*17*, *19*, *24*). MZ B cells transport Ag to B cell follicles to increase the efficiency of recognition by Ag-specific FO B cells (*25*). Trogocytic acquisition of DC receptors may expand their capacity for Ag capture and dissemination.

Notwithstanding the benefits trogocytosis may confer on MZ B cells, we have shown that this process must be limited to prevent cDC elimination. This notion is supported by the following observations: (i) Reductions in cDCs were only observed in mice where all three molecular components required for trogocytosis—MHC II, C3, and CR2—were present; (ii) cDCs were lost from the spleen, where MZ B cells are present, but not from lymph nodes, where MZ B cells are absent, even though cDCs displayed similar amounts of MHC II–C3 complexes in both locations; (iii) in mice that contained both *March1*$^{-/-}$ cDCs, which could act as a source of trogocytosed membrane, and wild-type cDCs, which could not, only the mutant cDCs were lost. We propose that wild-type cDCs can tolerate trogocytic sequestration of a small amount of plasma membrane but their mutant counterparts cannot repair the damage caused by enhanced trogocytosis and die by "trogoptosis" (*26*) (fig. S7). Reductions in cDCs may contribute to the described defects in T cell priming in *March1*$^{-/-}$ or MHC IIKR$^{KI/KI}$ mice (*3*, *14*).

MHC II ubiquitination by MARCH1 plays two important roles: to enhance the removal of surface MHC II–C3 complexes on all APCs, and, as described here, to limit MZ B cell trogocytosis and elimination of cDCs. It is conceivable that these two functions, more than the regulation of MHC II antigen presentation, have been the major drivers for the conservation of MHC II ubiquitination through evolution.

Materials and methods

Mice

Experimental wild-type C57BL/6, BALB/c, or C3H, and mutant *March*$^{-/-}$ (*27*), *C3*$^{-/-}$ (*28*) (The Jackson Laboratory 129S4-C3tm1Crr/J; #0036410), MHC IIKR$^{KI/KI}$ (*14*), *H2-Aa*$^{-/-}$ (*29*), and *Cr2*$^{-/-}$ (*30*) [The Jackson Laboratory 129S7(NOD)-Cr2tm1Hmo/J; #008225] mice were bred and maintained in specific pathogen-free conditions in the Melbourne Bioresources Platform at the Bio21 Molecular Science and Biotechnology Institute, Victoria, Australia. Analyses were undertaken with male and female mice aged 7 to 14 weeks and performed in accordance with the Institutional Animal Care and Use Committee guidelines of the University of Melbourne and the National Health and Medical Research Council of Australia, approved by the Animal Ethics Committee at the University of Melbourne (#1714238 and #1513472).

Isolation of primary murine cells and analysis by flow cytometry

Whole splenocyte suspensions were generated through digestion of finely chopped spleens with 0.1% DNase I (Roche) and collagenase type III (1 mg/ml; Worthington) followed by lysis of red blood cells through incubation with 168 mM ammonium chloride (5 min at room temperature). cDCs were purified from whole splenocyte suspensions as described (*31*). In brief, low-density splenocytes were

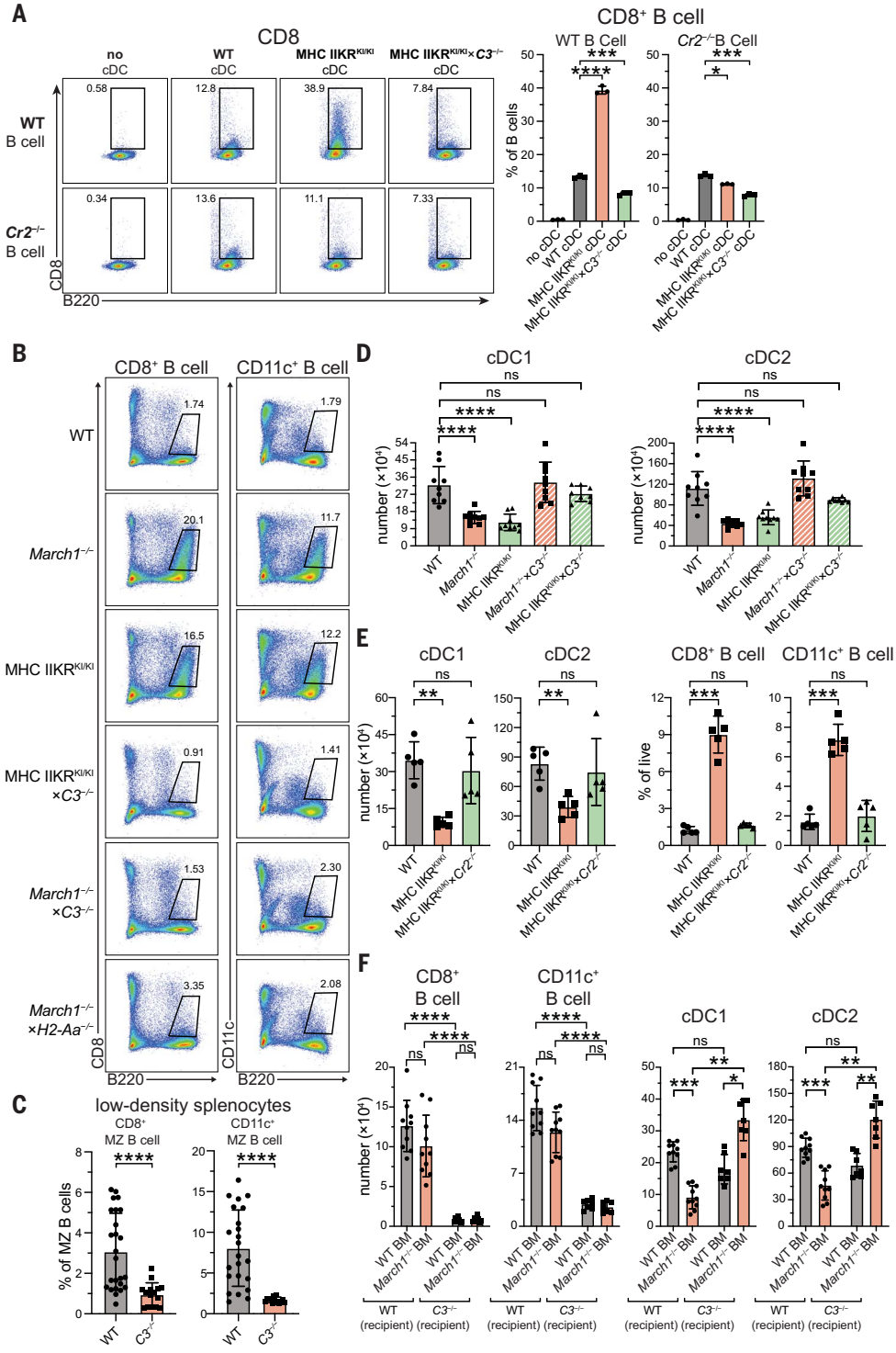

Fig. 7. B cell trogocytosis of cDC membrane is MHC II–, C3-, and CR2-dependent. (**A**) Trogocytic acquisition of CD8 from cDCs by wild-type or *Cr2*$^{-/-}$ B cells after their incubation with wild-type or mutant cDCs as indicated, with bar graphs (right) representing the percentage of CD8^{+} B cells, determined as shown in the flow cytometry plots (left). Each data point represents the measurement of a technical replicate (n = 3), displayed as mean ± SD. *P < 0.0332, ***P < 0.0002, ****P < 0.0001 [Welch's ANOVA test (no assumption of equal variances) followed by Games-Howell multiple-comparisons test, adjusted P value (95% CI)]. (**B**) Representative B220 versus CD8 and CD11c plots of flow cytometry analysis of low-density splenocytes from the indicated wild-type or mutant mice, showing the proportion of trogocytic (CD8^{+} and CD11c^{+}) B cells. Plots are representative of at least two independent experiments with two or three individual mice per experiment. (**C**) Frequency of trogocytic MZ B cells among low-density splenocytes of wild-type or *C3*$^{-/-}$ mice. (**D**) Number of splenic cDC1s and cDC2s in the indicated wild-type or mutant mice. (**E**) Number of cDC1s and cDC2s (left) and frequency of trogocytic B cells (right) identified as shown in (B) in the indicated wild-type or mutant mice. (**F**) Number of wild-type or *March1*$^{-/-}$ trogocytic B cells, cDC1s, and cDC2s present in the spleens of mixed-BM chimeras (wild-type or *C3*$^{-/-}$ recipient mice), reconstituted with a 1:1 mix of wild-type and *March1*$^{-/-}$ BM. Graphs in (C) to (F) display data pooled from six (C) or two [(D) to (F)] independent experiments, with each symbol representing an individual mouse (n = 2 to 5 per experiment); bars denote mean ± SD. *P < 0.0332, **P < 0.002, ***P < 0.0002, ****P < 0.0001 [independent-samples t test with Welch's correction (no assumption of equal variances) in (C), Welch's ANOVA test (no assumption of equal variances) followed by Games-Howell multiple-comparisons test in (D) and (E), or followed by pairwise comparison in (F), two-tailed (C), or adjusted [(D) to (F)] P value (all 95% CI)].

enriched by density gradient centrifugation (at 2237*g*) with 1.077 g/cm^3 Nycodenz (Axis shield) and subsequent negative depletion using rat mAbs against CD3 (KT3-1.1), Thy1 (T24/31.7), Ly-76 (Ter119), B220 (RA3-6B2), and Ly-6C/G (RB6-8C5) and BioMag anti-rat IgG-coupled magnetic beads (20 µl/10^6 cells, Qiagen), resulting in 75 to 90% purity. Similarly, cDCs from total lymph nodes were enriched through enzymatic digestion [0.1% DNase I and collagenase type III (1 mg/ml)] and Nycodenz (1.077 g/cm^3, Axis shield) gradient centrifugation (at 2237*g*). Splenic B cells were isolated from whole-splenocyte suspensions through gradient centrifugation (at 2237*g*) with Ficoll-Paque Plus (GE Healthcare) and subsequent negative depletion using FITC-conjugated mAb against CD4 (GK1.5, 1.6 µg/ml), Ly76 (TER119, 1.6 µg/ml), and CD43 (S7, 1.6 µg/ml) and magnetic anti-FITC MicroBeads (2 µl/10^6 cells, Miltenyi Biotec), resulting in 95 to 98% purity.

For flow cytometry analysis, purified murine cells were washed in EDTA-BSS with 2% (v/v) FCS, Fc receptor–blocked (1:50, Miltenyi Biotec), and incubated with mAb for the detection of surface markers (table S4). All

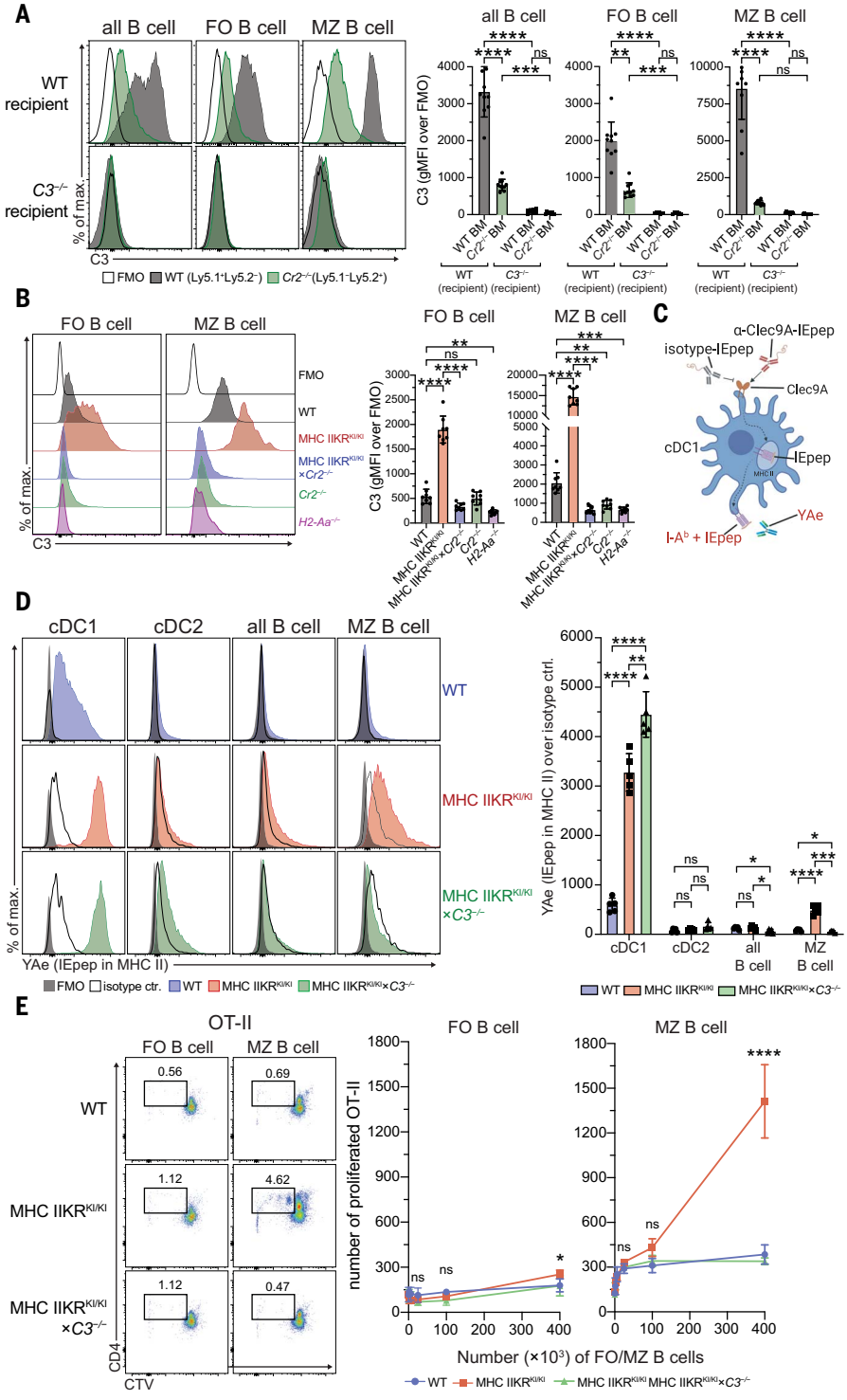

Fig. 8. MZ B cells present pMHC II complexes trogocytosed from cDC1s in vivo. (**A** and **B**) Representative flow cytometry histograms (left) and bar graphs with MFI values (right) of C3 surface expression on wild-type or $Cr2^{-/-}$ total, FO, or MZ B cells of mixed-BM chimera mice (wild-type or $C3^{-/-}$ recipients), reconstituted with a 1:1 mix of wild-type and $Cr2^{-/-}$ BM (A) or on FO and MZ B cells of the indicated wild-type or mutant mice (B). Bar graphs display data pooled from two independent experiments, with each symbol representing an individual mouse (n = 4 or 5 per experiment); bars denote mean ± SD. $^{**}P < 0.002$, $^{***}P < 0.0002$, $^{****}P < 0.0001$ [Welch's ANOVA test (no assumption of equal variances) followed by pairwise comparison (A) or by Games-Howell multiple-comparisons test (B), adjusted P value (95% CI)]. (**C**) Cartoon representing the capture of anti-Clec9A mAb fused to the I-E peptide (I-$Ea_{46\text{-}72}$) by cDC1s, followed by intracellular processing and presentation of I-E peptide by MHC II (I-A^b) and detection of the complex on the cell surface with YAe mAb. (**D**) Left: Surface expression of I-A^b + IEpep (YAe) on splenic cDC1s, cDC2s, total B cells, and MZ B cells of the indicated wild-type or mutant mice immunized with anti–Clec9A-IEpep or control isotype-IEpep mAb. Right: Bar graphs with MFI values of YAe surface expression; data pooled from two independent experiments, with each symbol representing an individual mouse (n = 2 or 3 per experiment), displayed as means ± SD. $^{*}P < 0.0332$, $^{**}P < 0.002$, $^{***}P < 0.0002$, $^{****}P < 0.0001$ [Welch's ANOVA test (no assumption of equal variances) followed by pairwise comparison within each group (cell type), P value (all 95% CI)]. (**E**) Proliferation of OT-II cells incubated with increasing numbers of sort-purified FO or MZ B cells from the indicated wild-type or mutant mice immunized with anti-Clec9A mAb conjugated with OVA. Left: Dividing OT-II cells, gated as shown in the representative flow cytometry plots. Right: Numbers of proliferated OT-II cells pooled from two independent experiments, with each symbol representing a technical replicate (n = 3 per experiment), displayed as means ± SD. $^{*}P < 0.0332$, $^{****}P < 0.0001$ (one-way ANOVA followed by Bonferroni's multiple-comparisons test).

fluorescence-minus-one (FMO) controls correspond to cells that were stained with mAbs for the detection of lineage markers but not for the indicated molecule. Cell surface C3 was detected using biotinylated anti-C3 mAbs clone 11H9 (Novus Biological), clone 3d29 [kindly provided by V. M. Holers and J. M. Thurman, School of Medicine, University of Colorado, Denver, Anschutz Medical Campus (*32*)], or polyclonal Abs (pAbs) HP8012 (Hycult) and 55500 (MP Biomedical) (table S4) with subsequent incubation with BV605-, APC-, or APCCy7-conjugated streptavidin. All FMO controls for C3 surface staining correspond to cells that were incubated with mAbs for the detection of lineage markers, including streptavidin-BV605/APC-Cy7/APC but no biotinylated anti-C3 Abs. All staining steps were performed on ice (30 min) and isotype-matched control Abs were used where required. Cells were analyzed using a LSRFortessa flow cytometer (BD Biosciences) in the Melbourne Cytometry Platform (University of Melbourne) and FlowJo software (Tree Star) with exclusion of cell doublets and dead cells, in all cases identified on the basis of forward and side scatter (FSC and SSC) and propidium iodide (PI) staining (fig. S2).

Enumeration of cells via flow cytometry was performed using a defined number of Sphero blank calibration beads (BD BioSciences).

B cells were identified as $CD19^+B220^+$, $CD4^+$ T cells as $CD3^+CD4^+$, $CD8^+$ T cells as $CD3^+CD8^+$, pDCs as MHC $II^+CD11c^+BST\text{-}2^+$Siglec H^+, and cDCs as $CD11c^+$MHC II^+, with further discrimination of cDC1s as $CD11b^-CD8^+$ and cDC2s as $CD11b^+CD8^-$ (fig. S2). Macrophages were identified as $F4/80^+CD64^+$, neutrophils as $B220^-CD3^-CD4^-CD8^-CD11c^{lo\text{-}int}CD11b^{hi}Ly6G^+$, and eosinophils as $B220^-CD3^-CD4^-CD8^-CD11c^{lo\text{-}int}CD11b^{hi}Ly6G^-$SSC-$H^{hi}Ly6C^{lo\text{-}int}$ (*33*).

Isolation of human blood DCs and analysis by flow cytometry

Blood samples from healthy donors (n = 10, male and female, 45.8 ± 15.9 years of age) were obtained as buffy coats from the Australian Red Cross Lifeblood, Victoria, Australia, with written and informed consent from the donors and ethics approval from the University of Melbourne Human Research and Ethics Committee (#1035100). Whole blood samples from MHC II–deficient patients (n = 2, male, 11 and 15 years of age) were collected by staff of the Royal Children's Hospital, Victoria, Australia, with written and informed consent from the donors and ethics approval from the Royal Children's Hospital Research Ethics Committee (#33146) after receiving regular intravenous immunoglobulin (IVIg) infusions. Peripheral blood mononuclear cells (PBMCs) from both healthy donors as well as from MHC II–deficient patients were enriched using centrifugation (at 2237*g*) with Ficoll-Paque Plus (GE Healthcare). DCs were purified from PBMCs with the Pan-DC Enrichment Kit (Miltenyi Biotec) according to the manufacturer's instructions. In brief, 10^8 cells were stained with mAb to block FcR and incubated with a depletion Ab cocktail and magnetic microbeads to deplete Ab-labeled cells using LS magnetic columns and MidiMACS magnet (both Miltenyi Biotec). This resulted in 5 to 10% purity of cDCs ($CD11c^+$HLA-DR^+). For flow cytometry analysis, purified human DCs were washed in EDTA-BSS with 2% (v/v) FCS and incubated with mAb against CD1c (L161), CD11c (3.9), CD141 (M80), HLA-DR (LN3), CD123 (6H6), or lineage (lin) mAb cocktail against CD3, CD14, CD16, CD19, CD20, and CD56 (OKT3, M5E2, 3G8, HIB19, 2H7, and HCD56). cDC1s were identified as $lin^-CD11c^{int\text{-}hi}CD123^-CD141^+CD1c^-$, cDC2s as $lin^-CD11c^{int\text{-}hi}CD123^-CD141^-CD1c^+$, and pDCs as $lin^-CD11c^{int\text{-}hi}CD11b^-CD123^+$ (fig. S5B). Cells were incubated with whole rabbit serum and cell surface C3 detected using biotinylated anti-C3–specific rabbit pAb (Abcam, ab48342) with subsequent incubation with APC-conjugated streptavidin, including appropriate controls to ensure specificity (fig. S5C). Cells were analyzed using an LSRFortessa (BD Biosciences) and FlowJo software (Tree Star) with exclusion of cell doublets and dead cells in all cases identified on the basis of FSC and SSC and staining with PI.

RNA sequencing and transcriptomic analysis

Splenic cDC1s, B cells, and $CD11c^{int}CD24^+CD8^{int}$ cells from four biological replicates with pooled spleens from five wild-type or *March1*$^{-/-}$ mice per replicate were sorted (95 to 99% purity) with the Influx Cell Sorter (BD Biosciences) at Murdoch Children's Research Institute, Royal Children's Hospital, Victoria, Australia. Genomic DNA was removed and total RNA extracted using the RNeasy Mini Kit (Qiagen). RNA quality was assessed via Agilent Bioanalyzer 2100 using the Agilent RNA 6000 Nano Kit (Agilent Technologies) and rRNA depletion and library preparation were performed according to manufacturer protocols (TruSeq, Illumina) at the Australian Genome Research Facility (AGRF), Victoria, Australia. Whole-transcriptome sequencing was undertaken using Illumina Hi Seq 2500 (Illumina, San Diego, CA) at the AGRF in replicates on two lanes. All 100–base pair single-end reads were mapped to the reference mouse genome (GRCm38/mm10) using STAR aligner (version 2.7) (*34*), and gene-wise counts were obtained using Subread package (v1.6.2) (*35*). Differential expression analysis of RNA sequencing data was carried out in Galaxy/Australia (usegalaxy.org.au, Melbourne Bioinformatics) (*36*) using the differential expression tool (Trinity assembly) (*37*, *38*) and in RStudio (version 1.1.447)/R (version 3.6.1) using the edgeR (version 3.26.6) (*39*) and limma (version 3.40.2) (*40*) packages. Gene counts were converted to $\log_2$ counts per million and normalized using the trimmed mean of M-values normalization method in edgeR (*41*). Precision weights were applied with the "voom" function (*42*) of the limma package, and a linear model was fitted to each gene correcting for inter-replicate variation. Empirical Bayes-moderated t statistics were used to assess differences in gene expression and determine P values. Differences in expression levels were evaluated using a linear model on replicates, with samples compared across the different groups. Genes were corrected for multiple testing, and genes having a false discovery rate (FDR) of <0.05 using the decideTest function (*43*) in limma were considered significant. Gene set analysis was performed using the fast implementation of rotation gene set testing (*44*) (FRY in limma) for B cell signatures—GO:0042113 for B cell activation and BCR signaling pathway (Biocarta) from the Molecular Signatures Database (org.Mm.eg.db version 3.12.0). RNA-seq data from this study were deposited in GEO under accession number 185597.

In vitro trogocytosis assay

In vitro trogocytosis assays were carried out as described (*9*), excluding Ag priming. In brief, 2×10^5 B cells and 3×10^5 cDCs purified from spleens were cocultured in RPMI media supplemented with 10% (v/v) FCS (Sigma), 1× GlutaMAX (Gibco), penicillin (100 U/ml), streptomycin (100 μg/ml; Media Preparation Unit, Peter Doherty Institute, Victoria, Australia), and 50 μM β-mercaptoethanol (Life Technologies) in 96-well U-bottom cell culture plates for 2 hours at 37°C after quick centrifugation at 150*g* to promote cell contact. In some experiments, either cDCs or B cells were stained with PKH26 Red Fluorescent Cell Linker according to the manufacturer's instructions (Sigma Aldrich). After incubation, cells were washed in EDTA-BSS with 2% (v/v) FCS to disrupt intercellular clusters and analyzed by flow cytometry as described above.

Mixed–bone marrow chimeric mice

Bone marrow (BM) was harvested from tibia and femur of donor mice (wild-type, *March1*$^{-/-}$, and *Cr2*$^{-/-}$), and recipient mice (wild-type and *C3*$^{-/-}$) were irradiated twice at 550 cGy (rad), 3 hours apart, before intravenously injected with 50:50 mixed BM cells. Recipient mice were intraperitoneally injected with anti-Thy1 (clone T24) to eliminate radio-resistant host T cells the day after irradiation. Mice were reconstituted for at least 8 weeks before use.

Immunoblotting, immunoprecipitation, and PNGase F treatment of MHC II and C3

cDCs purified from Flt3L-expanded mice (*45*) were lysed on ice in 1% (v/v) IGEPAL CA-630 (Sigma-Aldrich), 50 mM Tris (pH 7.5; Astral Scientific), 5 mM magnesium chloride (Chem-Supply), and cOmplete protease inhibitor cocktail (Roche) at a concentration of 10^7 cells/ml, and nuclei were removed by centrifugation at 14,000*g* at 4°C. For immunoprecipitation of MHC II and C3, lysates were precleared twice by incubation with uncoupled protein G–sepharose beads (Walter and Eliza Hall Institute, WEHI) in the presence of normal rabbit serum. To immunoprecipitate MHC II or C3, protein G–sepharose beads were precoupled with anti–I-A/I-E (clone M5/115) mAb (10 μg per 10^7 cells) or anti-C3dg (clone 3d29) mAb (5 μg per 10^7 cells) and added to the lysate. To eluate MHC II/C3 from protein G–sepharose beads for immunoblot analysis, beads were incubated in 3× SDS (reducing) sample buffer at 95°C. For deglycosylation of MHC II molecules, treatment with PNGase F was carried out according to manufacturer's instructions (New England BioLabs). In brief, washed protein G–sepharose beads with mAb-bound MHC II molecules were incubated with denaturing buffer followed by incubation with 500 U of PNgase F in 1× GlycoBuffer containing 1% NP-40.

For analysis of MHC II and C3 by immunoblotting, serum samples, whole-cell lysates or immunoprecipitates from equal cell numbers were separated on a precast NuPAGE gel (4 to

12% Bis-Tris Plus) and transferred to iBlot 2 PVDF membranes with an iBlot 2 system according to manufacturer's instructions (all Invitrogen). Samples were probed for C3 with anti-C3 pAb from rabbit serum (HP8012, Hycult) or MHC II with anti–I-Aα– or anti–I-Aβ–specific pAb from rabbit serum JV1 and JV2 (WEHI antibody facility) followed by HRP-coupled secondary antibodies with the appropriate species reactivities. Chemiluminescence was measured using the ECL Select Western Blotting reagent (Amersham GE Healthcare), acquired on a ChemiDoc MP imaging system (Bio-Rad) and ImageJ.

Mass spectrometry

Immunoprecipitated MHC II was analyzed using a precast NuPAGE gel (4 to 12% Bis-Tris Plus, Invitrogen) and stained using Coomassie Brilliant Blue R-250 (Bio-Rad). Bands of interest were excised and subjected to reduction, alkylation, and trypsin digestion before mass spectrometry (MS) as described (*46*). In brief, excised gel samples were destained in 50 mM ammonium bicarbonate dissolved in 50% (v/v) acetonitrile, reduced with 10 mM dithiothreitol (DTT), and then alkalized with 55 mM iodoacetamide. Air-dried gel pieces were incubated with trypsin (15 ng/μl, Promega) in 25 mM ammonium bicarbonate for ~16 hours at 37°C and peptides were extracted through incubation with 0.1% (v/v) formic acid in 60% acetonitrile.

Mass spectrometry and data analysis were carried out at the WEHI Proteomic Laboratory (Webb laboratory), Victoria, Australia. Extracted peptides were separated by reverse-phase chromatography on a 1.9-μm C18 fused silica column (I.D. 75 μm, O.D. 360 μm × 25 cm length) packed into an emitter tip (Ion Opticks, Australia), using a nano-flow HPLC (M-class, Waters). The HPLC was coupled to an Impact II UHR-QqTOF mass spectrometer (Bruker) using a CaptiveSpray source and nanoBooster at 0.20 bar using acetonitrile. Peptides were loaded directly onto the column at a constant flow rate of 400 nl/min with buffer A (99.9% Milli-Q water, 0.1% formic acid) and eluted with a 90-min linear gradient from 2 to 34% buffer B (99.9% acetonitrile, 0.1% formic acid). Mass spectra were acquired in a data-dependent manner including an automatic switch between MS and MS/MS scans using a 1.5-s duty cycle and 4-Hz MS1 spectra rate followed by MS/MS scans at 8 to 20 Hz dependent on precursor intensity for the remainder of the cycle. MS spectra were acquired within a mass range of 200 to 2000 *m/z*. Peptide fragmentation was performed using collision-induced dissociation (CID).

All raw files were analyzed by MaxQuant (1.5.6.5) software using the integrated Andromeda search engine. Experiment type was set as TIMS-DDA with no modification to default settings. Data were searched against the mouse Uniprot Reference Proteome with isoforms and a separate reverse decoy database using a strict trypsin specificity allowing up to two missed cleavages. The minimum required peptide length was seven amino acids.

Immunization with IEpep/OVA-conjugated Clec9A mAb for YAe detection and ex vivo antigen presentation assay

IEpep ($Ea_{52\text{-}68}$)–loaded I-Ab surface expression, as detected by biotinylated YAe mAb (*16*) (Thermo Fisher), was analyzed at the surface of cDCs and B cells after intravenous injection of mice with 0.5 μg of anti–Clec9A-IEpep (clone 10B4) (*47*) or isotype-IEpep mAb. The IEa epitope ($I\text{-}Ea_{46\text{-}72}$) was cloned in-frame with the heavy chain C terminal region of the Clec9A mAb (clone 10B4) or isotype mAb via alanine linkers. After 22 to 24 hours, splenic cDCs and B cells were examined for IEpep ($Ea_{52\text{-}68}$)–loaded I-Ab surface expression by flow cytometry using biotinylated YAe mAb and streptavidin-PE. FMO controls for YAe surface staining correspond to cells that were incubated with mAb for the detection of lineage markers, including streptavidin-PE but not biotinylated YAe mAb.

For ex vivo antigen presentation assays, mice were intravenously injected with 1 μg of Clec9A-OVA mAb. After 22 to 24 hours, spleen MZ and follicular (FO) B cells were sorted to purity. OT-II cells were purified from lymph nodes and labeled with 2 μM CellTrace Violet (CTV), and 5×10^4 cells per well were cultured with isolated FO or MZ B cells in U-bottom 96-well plates for 90 hours. Proliferated OT-II cells were determined by flow cytometry as the number of $CD4^+TCRV\alpha2^+$ cells that had undergone CTV dilution.

REFERENCES AND NOTES

1. J. A. Villadangos, Presentation of antigens by MHC class II molecules: Getting the most out of them. *Mol. Immunol.* **38**, 329–346 (2001). doi: 10.1016/S0161-5890(01)00069-4; pmid: 11684289
2. H. Liu, J. D. Mintern, J. A. Villadangos, MARCH ligases in immunity. *Curr. Opin. Immunol.* **58**, 38–43 (2019). doi: 10.1016/j.coi.2019.03.001; pmid: 31063934
3. K. R. Wilson *et al*., MARCH1-mediated ubiquitination of MHC II impacts the MHC I antigen presentation pathway. *PLOS ONE* **13**, e0200540 (2018). doi: 10.1371/journal.pone.0200540; pmid: 30001419
4. H. J. Kim *et al*., Ubiquitination of MHC Class II by March-I Regulates Dendritic Cell Fitness. *J. Immunol.* **206**, 494–504 (2021). doi: 10.4049/jimmunol.2000975; pmid: 33318291
5. V. M. Holers, Complement and its receptors: New insights into human disease. *Annu. Rev. Immunol.* **32**, 433–459 (2014). doi: 10.1146/annurev-immunol-032713-120154; pmid: 24499275
6. M. K. Pangburn, V. P. Ferreira, C. Cortes, Discrimination between host and pathogens by the complement system. *Vaccine* **26** (Suppl 8), I15–I21 (2008). doi: 10.1016/j.vaccine.2008.11.023; pmid: 19388159
7. F. Bexborn, P. O. Andersson, H. Chen, B. Nilsson, K. N. Ekdahl, The tick-over theory revisited: Formation and regulation of the soluble alternative complement C3 convertase ($C_3(H_2O)Bb$). *Mol. Immunol.* **45**, 2370–2379 (2008). doi: 10.1016/j.molimm.2007.11.003; pmid: 18096230
8. A. Cerutti, M. Cols, I. Puga, Marginal zone B cells: Virtues of innate-like antibody-producing lymphocytes. *Nat. Rev. Immunol.* **13**, 118–132 (2013). doi: 10.1038/nri3383; pmid: 23348416
9. S. Daubeuf, A.-L. Puaux, E. Joly, D. Hudrisier, A simple trogocytosis-based method to detect, quantify, characterize and purify antigen-specific live lymphocytes by flow cytometry, via their capture of membrane fragments from antigen-presenting cells. *Nat. Protoc.* **1**, 2536–2542 (2006). doi: 10.1038/nprot.2006.400; pmid: 17406507
10. E. Joly, D. Hudrisier, What is trogocytosis and what is its purpose? *Nat. Immunol.* **4**, 815–815 (2003). doi: 10.1038/ni0903-815; pmid: 12942076
11. D. M. Davis, Intercellular transfer of cell-surface proteins is common and can affect many stages of an immune response. *Nat. Rev. Immunol.* **7**, 238–243 (2007). doi: 10.1038/nri2020; pmid: 17290299
12. P. Schriek *et al*., Physiological substrates and ontogeny-specific expression of the ubiquitin ligases MARCH1 and MARCH8. *Curr. Res. Immunol.* **2**, 218–228 (2021). doi: 10.1016/j.crimmu.2021.10.004
13. Z. Zhou, M.-J. Xu, B. Gao, Hepatocytes: A key cell type for innate immunity. *Cell. Mol. Immunol.* **13**, 301–315 (2016). doi: 10.1038/cmi.2015.97; pmid: 26685902
14. M. Ohmura-Hoshino *et al*., Cutting edge: Requirement of MARCH-I-mediated MHC II ubiquitination for the maintenance of conventional dendritic cells. *J. Immunol.* **183**, 6893–6897 (2009). doi: 10.4049/jimmunol.0902178; pmid: 19917682
15. W. Wiszniewski *et al*., Novel mutations in the RFXANK gene: RFX complex containing in-vitro-generated RFXANK mutant binds the promoter without transactivating MHC II. *Immunogenetics* **54**, 747–755 (2003). doi: 10.1007/s00251-002-0521-1; pmid: 12618906
16. Rudensky AYu, S. Rath, P. Preston-Hurlburt, D. B. Murphy, C. A. Janeway Jr., On the complexity of self. *Nature* **353**, 660–662 (1991). doi: 10.1038/353660a0; pmid: 1656278
17. I. Caminschi *et al*., The dendritic cell subtype-restricted C-type lectin Clec9A is a target for vaccine enhancement. *Blood* **112**, 3264–3273 (2008). doi: 10.1182/blood-2008-05-155176; pmid: 18669894
18. J. Banchereau, R. M. Steinman, Dendritic cells and the control of immunity. *Nature* **392**, 245–252 (1998). doi: 10.1038/32588; pmid: 9521319
19. W. R. Heath, Y. Kato, T. M. Steiner, I. Caminschi, Antigen presentation by dendritic cells for B cell activation. *Curr. Opin. Immunol.* **58**, 44–52 (2019). doi: 10.1016/j.coi.2019.04.003; pmid: 31071588
20. J. F. Kearney, P. Patel, E. K. Stefanov, R. G. King, Natural antibody repertoires: Development and functional role in inhibiting allergic airway disease. *Annu. Rev. Immunol.* **33**, 475–504 (2015). doi: 10.1146/annurev-immunol-032713-120140; pmid: 25622195
21. H. Liu *et al*., Ubiquitination of MHC Class II Is Required for Development of Regulatory but Not Conventional $CD4^+$ T Cells. *J. Immunol.* **205**, 1207–1216 (2020). doi: 10.4049/jimmunol.1901328; pmid: 32747505
22. S. J. Swiedler, G. W. Hart, A. L. Tarentino, T. H. Plummer Jr., J. H. Freed, Stable oligosaccharide microheterogeneity at individual glycosylation sites of a murine major histocompatibility antigen derived from a B-cell lymphoma. *J. Biol. Chem.* **258**, 11515–11523 (1983). doi: 10.1016/S0021-9258(17)44258-X; pmid: 6604728
23. S. E. Cullen, C. S. Kindle, D. C. Shreffler, C. Cowing, Differential glycosylation of murine B cell and spleen adherent cell Ia antigens. *J. Immunol.* **127**, 1478–1484 (1981). pmid: 6792276
24. S. F. Gonzalez *et al*., Capture of influenza by medullary dendritic cells via SIGN-R1 is essential for humoral immunity in draining lymph nodes. *Nat. Immunol.* **11**, 427–434 (2010). doi: 10.1038/ni.1856; pmid: 20305659
25. G. Cinamon, M. A. Zachariah, O. M. Lam, F. W. Foss Jr., J. G. Cyster, Follicular shuttling of marginal zone B cells facilitates antigen transport. *Nat. Immunol.* **9**, 54–62 (2008). doi: 10.1038/ni1542; pmid: 18037889
26. H. L. Matlung *et al*., Neutrophils Kill Antibody-Opsonized Cancer Cells by Trogoptosis. *Cell Rep.* **23**, 3946–3959.e6 (2018). doi: 10.1016/j.celrep.2018.05.082; pmid: 29949776
27. Y. Matsuki *et al*., Novel regulation of MHC class II function in B cells. *EMBO J.* **26**, 846–854 (2007). doi: 10.1038/sj.emboj.7601556; pmid: 17255932
28. Q. Shi *et al*., Complement C3-Deficient Mice Fail to Display Age-Related Hippocampal Decline. *J. Neurosci.* **35**, 13029–13042 (2015). doi: 10.1523/JNEUROSCI.1698-15.2015; pmid: 26400934
29. F. Köntgen, G. Süss, C. Stewart, M. Steinmetz, H. Bluethmann, Targeted disruption of the MHC class II Aa gene in C57BL/6 mice. *Int. Immunol.* **5**, 957–964 (1993). doi: 10.1093/intimm/5.8.957; pmid: 8398989
30. H. Molina *et al*., Markedly impaired humoral immune response in mice deficient in complement receptors 1 and 2. *Proc. Natl.*

Acad. Sci. U.S.A. **93**, 3357–3361 (1996). doi: 10.1073/pnas.93.8.3357; pmid: 8622941
31. D. Vremec, K. Shortman, The isolation and identification of murine dendritic cell populations from lymphoid tissues and their production in culture. *Methods Mol. Biol.* **415**, 163–178 (2008). doi: 10.1007/978-1-59745-570-1_10; pmid: 18370154
32. J. M. Thurman *et al*., Detection of complement activation using monoclonal antibodies against C3d. *J. Clin. Invest.* **123**, 2218–2230 (2013). doi: 10.1172/JCI65861; pmid: 23619360
33. S. E. Liyanage *et al*., Flow cytometric analysis of inflammatory and resident myeloid populations in mouse ocular inflammatory models. *Exp. Eye Res.* **151**, 160–170 (2016). doi: 10.1016/j.exer.2016.08.007; pmid: 27544307
34. A. Dobin *et al*., STAR: Ultrafast universal RNA-seq aligner. *Bioinformatics* **29**, 15–21 (2013). doi: 10.1093/bioinformatics/bts635; pmid: 23104886
35. Y. Liao, G. K. Smyth, W. Shi, The Subread aligner: Fast, accurate and scalable read mapping by seed-and-vote. *Nucleic Acids Res.* **41**, e108–e108 (2013). doi: 10.1093/nar/gkt214; pmid: 23558742
36. E. Afgan *et al*., The Galaxy platform for accessible, reproducible and collaborative biomedical analyses: 2018 update. *Nucleic Acids Res.* **46**, W537–W544 (2018). doi: 10.1093/nar/gky379; pmid: 29790989
37. D. Blankenberg, N. Coraor, G. Von Kuster, J. Taylor, A. Nekrutenko, Galaxy Team, Integrating diverse databases into an unified analysis framework: A Galaxy approach. *Database* **2011**, bar011–bar011 (2011). doi: 10.1093/database/bar011; pmid: 21531983
38. C. Sloggett, N. Goonasekera, E. Afgan, BioBlend: Automating pipeline analyses within Galaxy and CloudMan. *Bioinformatics* **29**, 1685–1686 (2013). doi: 10.1093/bioinformatics/btt199; pmid: 23630176
39. M. D. Robinson, D. J. McCarthy, G. K. Smyth, edgeR: A Bioconductor package for differential expression analysis of digital gene expression data. *Bioinformatics* **26**, 139–140 (2010). doi: 10.1093/bioinformatics/btp616; pmid: 19910308
40. M. E. Ritchie *et al*., limma powers differential expression analyses for RNA-sequencing and microarray studies. *Nucleic Acids Res.* **43**, e47 (2015). doi: 10.1093/nar/gkv007; pmid: 25605792
41. M. D. Robinson, A. Oshlack, A scaling normalization method for differential expression analysis of RNA-seq data. *Genome Biol.* **11**, R25 (2010). doi: 10.1186/gb-2010-11-3-r25; pmid: 20196867
42. C. W. Law, Y. Chen, W. Shi, G. K. Smyth, voom: Precision weights unlock linear model analysis tools for RNA-seq read counts. *Genome Biol.* **15**, R29 (2014). doi: 10.1186/gb-2014-15-2-r29; pmid: 24485249
43. C. W. Law *et al*., RNA-seq analysis is easy as 1-2-3 with limma, Glimma and edgeR. *F1000 Res.* **5**, 1408 (2016). doi: 10.12688/f1000research.9005.3; pmid: 27441086
44. D. Wu *et al*., ROAST: Rotation gene set tests for complex microarray experiments. *Bioinformatics* **26**, 2176–2182 (2010). doi: 10.1093/bioinformatics/btq401; pmid: 20610611
45. N. Mach *et al*., Differences in dendritic cells stimulated in vivo by tumors engineered to secrete granulocyte-macrophage colony-stimulating factor or Flt3-ligand. *Cancer Res.* **60**, 3239–3246 (2000). pmid: 10866317
46. J. R. Wiśniewski, A. Zougman, N. Nagaraj, M. Mann, Universal sample preparation method for proteome analysis. *Nat. Methods* **6**, 359–362 (2009). doi: 10.1038/nmeth.1322; pmid: 19377485
47. Y. Kato *et al*., Display of Native Antigen on cDC1 That Have Spatial Access to Both T and B Cells Underlies Efficient Humoral Vaccination. *J. Immunol.* **205**, 1842–1856 (2020). doi: 10.4049/jimmunol.2000549; pmid: 32839238

ACKNOWLEDGMENTS

We thank S. Choo (Royal Children's Hospital, Melbourne, Australia) for human blood samples; A. I. Webb, L. F. Dagley, and G. Infusini (Advanced Technology and Biology Division, Walter and Eliza Hall Institute of Medical Research, Melbourne, Australia) for the mass spectrometry analyses; and S. Finch for reviewing the statistical analyses. Schematics were created with BioRender.com. **Funding:** National Health and Medical Research Council of Australia 1058193 (J.A.V.), National Health and Medical Research Council of Australia 1016629 (W.R.H., J.A.V.), National Health and Medical Research Council of Australia 1113293 (W.R.H.), Australian Research Council DP110101383 (J.A.V.), Australian Research Council DP160103134 (J.A.V.), Human Frontier Science Program 0064/2011 (S.I., J.A.V.), National Health Institute R01 DK125823 (J.M.T., V.M.H.), NIH R01DK076690 (J.M.T.), and Australian Research Training Program Scholarship (P.S.). **Author contributions:** Conceptualization: J.A.V. Methodology: J.M.T., P.S., A.C.C., N.S.M., J.M., L.B., T.M.S., L.M.H., V.M.H., S.I., M.H.L., I.C., and W.R.H. Investigation: P.S., A.C.C., N.S.M., J.M., L.B., T.M.S., L.M.H., V.M.H., S.I., M.H.L., I.C., and W.R.H. Visualization: P.S., N.S.M., J.D.M., and J.A.V. Funding acquisition: W.R.H., S.I., and J.A.V. Project administration: J.A.V. Supervision: J.D.M. and J.A.V. Writing–original draft: P.S., J.D.M., and J.A.V. Writing–review and editing: P.S., J.D.M., and J.A.V. **Competing interests:** J.M.T. receives royalties from Alexion Pharmaceuticals Inc. and is a consultant for Q32 Bio Inc., a company developing complement inhibitors. He holds stock and will receive royalty income from Q32 Bio Inc. The authors declare no other competing interests. **Data and materials availability:** RNA-seq data from this study are deposited in GEO under accession number 185597. All other data needed to evaluate the conclusions in this paper are present in the manuscript or the supplementary materials. The *March1*$^{-/-}$ and MHC IIKR$^{KI/KI}$ mice used in this study were obtained from RIKEN Yokohama Institute under the terms of a materials transfer agreement (MTA) with the University of Melbourne. The anti-C3 antibodies were used under the terms of an MTA between the University of Colorado and the University of Melbourne. Patient samples were obtained under the terms of a research collaboration agreement between Melbourne Health and the University of Melbourne. Anti-Clec9A-IEpep and anti-Clec9A-OVA mAbs are available upon establishment of an MTA with Monash University.

SUPPLEMENTARY MATERIALS

science.org/doi/10.1126/science.abf7470
Figs. S1 to S7
Tables S1 to S4

17 November 2020; resubmitted 3 July 2021
Accepted 6 January 2022
10.1126/science.abf7470